IVYSPRING INTERNATIONAL PUBLISHER

Theranostics

2016; 6(12): 2267-2277. doi: 10.7150/thno.16744

Research Paper

A Pretargeted Approach for the Multimodal PET/NIRF Imaging of Colorectal Cancer

Pierre Adumeau[1], Kathryn E. Carnazza[2], Christian Brand[2], Sean D. Carlin[2], Thomas Reiner[2,3], Brian J. Agnew[4], Jason S. Lewis[2,3,5], Brian M. Zeglis[1,2,3,6]✉

1. Department of Chemistry, Hunter College of the City University of New York, New York, NY, 10028;
2. Department of Radiology, Memorial Sloan Kettering Cancer Center, New York, NY, 10065;
3. Department of Radiology, Weill Cornell Medical College, New York, NY, 10065;
4. Licensing and Commercial Supply, Thermo Fisher Scientific, Eugene, OR, 97402;
5. Program in Molecular Pharmacology and Chemistry, Memorial Sloan Kettering Cancer Center, New York, NY, 10065;
6. Ph.D. Program in Chemistry, the Graduate Center of the City University of New York, New York, NY, 10016.

✉ Corresponding author: Phone: 212-896-0443. Fax: 212-772-5332. E-mail: bz102@hunter.cuny.edu.

Received: 2016.07.06; Accepted: 2016.09.10; Published: 2016.09.28

Abstract

The complementary nature of positron emission tomography (PET) and near-infrared fluorescence (NIRF) imaging makes the development of strategies for the multimodal PET/NIRF imaging of cancer a very enticing prospect. Indeed, in the context of colorectal cancer, a single multimodal PET/NIRF imaging agent could be used to stage the disease, identify candidates for surgical intervention, and facilitate the image-guided resection of the disease. While antibodies have proven to be highly effective vectors for the delivery of radioisotopes and fluorophores to malignant tissues, the use of radioimmunoconjugates labeled with long-lived nuclides such as ^{89}Zr poses two important clinical complications: high radiation doses to the patient and the need for significant lag time between imaging and surgery. *In vivo* pretargeting strategies that decouple the targeting vector from the radioactivity at the time of injection have the potential to circumvent these issues by facilitating the use of positron-emitting radioisotopes with far shorter half-lives. Here, we report the synthesis, characterization, and *in vivo* validation of a pretargeted strategy for the multimodal PET and NIRF imaging of colorectal carcinoma. This approach is based on the rapid and bioorthogonal ligation between a *trans*-cyclooctene- and fluorophore-bearing immunoconjugate of the huA33 antibody (huA33-Dye800-TCO) and a ^{64}Cu-labeled tetrazine radioligand (^{64}Cu-Tz-SarAr). *In vivo* imaging experiments in mice bearing A33 antigen-expressing SW1222 colorectal cancer xenografts clearly demonstrate that this approach enables the non-invasive visualization of tumors *and* the image-guided resection of malignant tissue, all at only a fraction of the radiation dose created by a directly labeled radioimmunoconjugate. Additional *in vivo* experiments in peritoneal and patient-derived xenograft models of colorectal carcinoma reinforce the efficacy of this methodology and underscore its potential as an innovative and useful clinical tool.

Key words: PET, fluorescence imaging, multimodal imaging, colorectal carcinoma, pretargeting, bioorthogonal chemistry, site-specific bioconjugation.

Introduction

Colorectal cancer is the second most common malignancy in women, the third most common malignancy in men, and the fourth most common cause of cancer mortality worldwide.[1,2] In the US, the situation is even more dire, as this insidious disease is the third most common cause of cancer and the second most common cause of cancer mortality.[3] The surgical excision of the affected segments of the colon

has emerged as a standard of care for the treatment of colorectal cancer.[4] However, surgery is only effective in patients with localized disease. Patients with metastatic disease — who account for up to 25% of initial diagnoses — are not eligible for resection.[5,6] Not surprisingly, attempts at surgical intervention in these patients can actually be counter-productive, primarily because surgery can delay the start of chemotherapy.[7] Clearly, the accurate initial staging of colorectal carcinoma using rapid and non-invasive methods is absolutely essential to planning effective treatment regimens.

Over the past two decades, two imaging modalities have emerged that have begun to have a transformational impact on the clinical management of cancer. First, positron emission tomography (PET) — and immunoPET in particular — has become established as a powerful tool for the sensitive and specific functional imaging of cancer.[8] Second, near-infrared fluorescence (NIRF) imaging has proven to be a very promising technique for the image-guided resection of tumor tissue, as it facilitates the real-time, high-resolution delineation of tumor margins during surgery.[9,10] The complementary nature of these two modalities has led to a number of preclinical investigations focused on the creation of immunoconjugates for multimodal PET and NIRF imaging.[11–18] The hypothesis underpinning this work is that a single multimodal PET/NIRF imaging agent could perform two valuable functions. *Via* PET, the imaging agent could help clinicians non-invasively determine the extent of disease and, as a result, whether a given patient is a candidate for surgery. Then, if surgery *does* occur, the same probe could be used for intraoperative NIRF imaging, thereby aiding surgeons in the delineation of tumor margins and facilitating the more thorough resection of the disease. Hong *et al.*, for example, have recently developed a ^{89}Zr- and IRDye800CW-labeled immunoconjugate of the CD105-targeting antibody TCR105 for the multimodal PET and NIRF imaging of murine models of metastatic breast cancer.[15]

Despite the immense potential of multimodal PET/NIRF immunoconjugates, two principal obstacles stand in the way of their widespread clinical implementation. Both of these issues stem from the isotopes traditionally used to radiolabel antibodies. The multi-day circulation times of antibodies means that to be effective imaging agents, they must be labeled with radioisotopes with multi-day physical half-lives such as ^{89}Zr ($t_{1/2}$ ~ 3.2 days) or ^{124}I ($t_{1/2}$ ~ 4.2 days). The use of these long-lived isotopes creates an important clinical complication: high radiation doses to healthy organs. In the context of *multimodal* PET/NIRF imaging, a second issue arises. In order to eschew operations on radioactive patients, multiple days (or even weeks) would be required between imaging and surgery to allow the radioisotope to decay. Critically, it is possible that the cancer can spread during this delay, rendering the initial staging scans obsolete and casting the feasibility of surgery into doubt. The latter point is particularly germane in the context of malignancies with fast doubling rates, such as colorectal and ovarian cancer.

In vivo pretargeting approaches could circumvent these issues by harnessing the high specificity and affinity of radioimmunoconjugates while simultaneously avoiding their sluggish pharmacokinetics and high background doses.[19] To achieve this, pretargeting strategies decouple the antibody from the radioisotope at the time of injection and combine these two components within the body. In essence, the radioimmunoconjugate is synthesized at the *tumor itself. In vivo* radiolabeling strategies offer clear advantages over conventional radioimmunoconjugates, as they facilitate tumor imaging at earlier time points, enable the use of shorter-lived radionuclides [*e.g.*^{64}Cu ($t_{1/2}$ = 12.7 h) and ^{68}Ga ($t_{1/2}$ = 68 min) rather than ^{89}Zr or ^{124}I], and produce significant reductions in radiation dose rates to patients. In the past, several strategies — ranging from bispecific antibodies to systems based on the affinity between streptavidin and biotin — have been developed to facilitate the *in vivo* ligation of antibodies and radioligands.[19] However, these approaches have suffered from several drawbacks, including the immunogenicity of streptavidin-based immune-conjugates and the complexity and lack of versatility of bispecific antibodies.

Over the past five years, our laboratories and a handful of others have pioneered *in vivo* pretargeting strategies based on the extraordinarily rapid and bioorthogonal inverse electron demand Diels-Alder (IEDDA) reaction between tetrazine (Tz) and *trans*-cyclooctene (TCO) (*Figure 1A*).[20–27] Generally speaking, this approach employs two components — a tetrazine-based radioligand and a TCO-bearing immunoconjugate — and four facile steps: (1) the injection of the mAb-TCO conjugate; (2) a localization time period during which the antibody accumulates in the tumor and clears from the blood; (3) the injection of the radiolabeled tetrazine; and (4) the *in vivo* click ligation of the two components followed by the rapid excretion of excess radioligand.[23,28] Preclinical PET imaging studies in murine models of both colorectal and pancreatic cancer have clearly shown that this pretargeting methodology delivers high concentrations of radioactivity to tumor tissue at much earlier time points than directly radiolabeled antibodies, produces high tumor-to-background

activity concentration ratios, and significantly reduces the overall radiation burden to the patient compared to analogous traditional radioimmunoconjugates.[28,29]

We contend that a pretargeted approach to multimodal PET/NIRF imaging would solve both of the issues that threaten to limit traditional multimodal radioimmunoconjugates: it would (1) dramatically lower the radiation dose to healthy tissues and (2) significantly reduce the requisite lag time between PET imaging and surgical intervention. To this end, we have developed a pretargeted multimodal PET/NIRF imaging agent based on an immunoconjugate of the huA33 antibody labeled with both a near-IR fluorophore (Dye800) and TCO (huA33-Dye800-TCO) and a ^{64}Cu-labeled tetrazine radioligand (^{64}Cu-Tz-SarAr) (*Figs. 1B and 2*). We report that this approach enables the rapid and non-invasive visualization of tumor tissue with excellent tumor-to-background activity concentration ratios. Furthermore, simulated tumor resections using a NIRF camera clearly demonstrate that this approach could be a very powerful tool for the real-time delineation of malignant tissue during image-guided surgery. Ultimately, we believe that this ^{64}Cu-based system offers a dramatic improvement over multimodal PET/NIRF radioimmunoconjugates synthesized using traditional, direct-labeling methodologies.

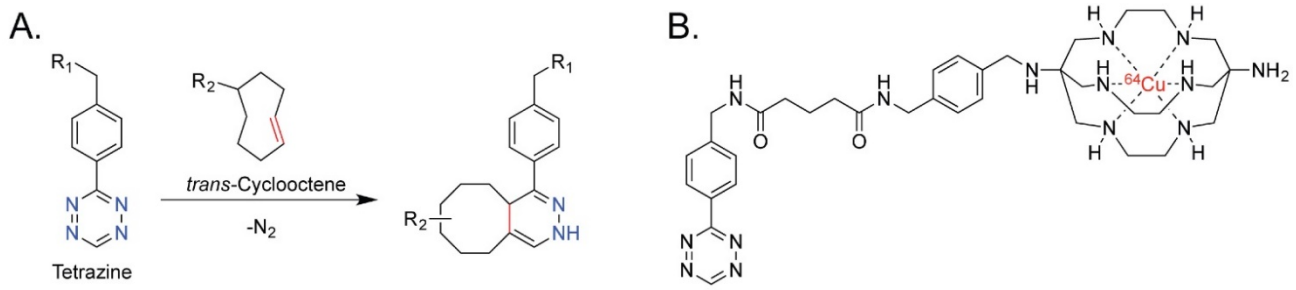

Figure 1. (A) The inverse electron demand Diels-Alder reaction between tetrazine and *trans*-cyclooctene; (B) ^{64}Cu-Tz-SarAr.

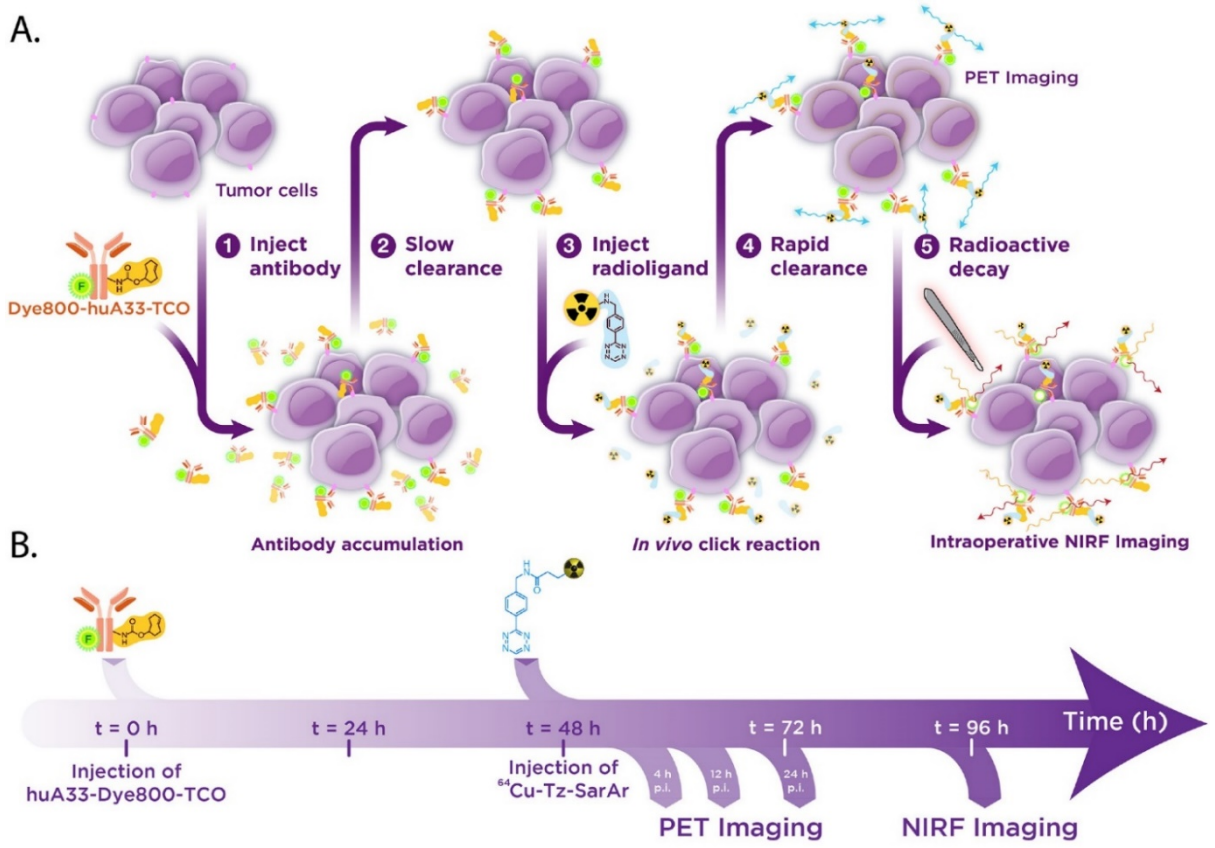

Figure 2. Biochemical (A) and temporal (B) schematics of the bioorthogonal pretargeting strategy for multimodal PET and NIRF imaging.

Materials and Methods

A detailed description of experimental procedures — including synthetic protocols, bioconjugation techniques, radiolabeling methodologies, and the design and execution of *in vitro* and *in vivo* experiments — can be found in the Supplementary Materials.

Results and Discussion

Design, Synthesis, and Characterization

The foundation of our multimodal imaging system lies in the pretargeted approach to the PET imaging of colorectal cancer that we have previously reported.[27,28] This approach pairs a ^{64}Cu-sarcophagine-based tetrazine radioligand (^{64}Cu-Tz-SarAr) with a TCO-labeled immunoconjugate of the huA33 antibody (huA33-TCO).[28] This antibody has previously been shown to be an excellent targeting vector for the A33 antigen, a glycoprotein biomarker that is over-expressed by 95% of colorectal carcinomas.[30–34] Critically, *in vitro* studies have shown that the huA33-A33 antigen complex is not internalized and persists on the surface of the cell for days after its formation, making this antibody-antigen pair an ideal platform for *in vivo* pretargeting.[35] The near-infrared dye IRDye®800CW (Dye800) was selected as the fluorescent reporter for this system for three reasons: it emits tissue-penetrating 789 nm light, it has been approved for clinical applications, and it has been successfully employed in several dual-labeled PET/NIRF immunoconjugates.[12,14–17]

Two different bioconjugation approaches were used to append the TCO and Dye800 moieties to the antibody in order to achieve maximum functionalization with minimal impairment of the antibody's functionality. The NIR fluorophore was attached first. To this end, we employed a chemoenzymatic strategy that site-specifically appends cargoes to the biantennary heavy chain glycans located on the C_H2 domains of the antibody's F_c region.[36] This methodology is designed to mitigate the adverse effects that the random attachment of cargoes can have on the immunoreactivity and pharmacokinetic profile of immunoconjugates. Indeed, a number of different studies have demonstrated that site-specifically labeled immunoconjugates are not only more homogenous and better-defined than their randomly labeled cousins but also often boast superior *in vivo* performance.[36–39] Along these lines, we have previously applied this bioconjugation strategy to the development of huA33-based multimodal imaging agents; however, in this case, we observed that the site-specifically modified constructs possess almost identical — if not *slightly* more favorable — *in vivo* behavior compared to their traditionally synthesized cousins.[18] This result is almost certainly a consequence of the well-optimized and robust nature of the huA33 antibody. Nonetheless, for the investigation at hand, we chose to employ this site-specific approach in order to *guarantee* that we have minimized the influence of the bulky and hydrophobic Dye800 on the *in vitro* and *in vivo* performance of the TCO-decorated antibody.

This site-specific bioconjugation strategy involves three steps: (1) the removal of the terminal galactose residues of the glycans using β-1,4-galactosidase; (2) the attachment of azide-modified monosaccharides (GalNAz) to the glycans using Gal-T1(Y289L), a promiscuous galactosyltransferase; and (3) the ligation of dibenzocyclooctyne-bearing derivatives of Dye800 (DIBO-Dye800) to the azide-terminated sugar chains via the strain-promoted azide-alkyne click (SPAAC) ligation (*Fig. 3*).[40–43] Interestingly, UV-Vis measurements revealed that the huA33-Dye800 immunoconjugate had a degree of labeling of 1.1 ± 0.1 Dye800/mAb. This ratio is admittedly lower than the theoretical maximum, given that the biantennary structure of the glycans means that a degree of labeling of 4 is possible. Indeed, degrees of labeling closer to 4 have been obtained using chelators (*e.g.* DIBO-DFO) and other, shorter-wavelength dyes (*e.g.* DIBO-AlexaFluor® 488).[18,44] However, this lower value is consistent with results previously obtained using a DIBO construct labeled with another bulky and hydrophobic NIRF dye, AlexaFluor™ 680 (AF680): 1.6 ± 0.2 AF680/mAb.[18] Efforts at understanding this phenomenon are currently underway, though at present we hypothesize that this reduction in reaction efficiency may best be explained by the steric hindrance produced by the introduction of a bulky and hydrophobic fluorophore with a large hydrodynamic radius.

The site specificity of this bioconjugation procedure was demonstrated via denaturing gel electrophoresis experiments performed on huA33-Dye800 and huA33-Dye800-TCO (*vide infra*) before and after treatment with PNGaseF, an endoglycosidase known to efficiently cleave the *N*-linked oligosaccharides from the C_H2 domains. Importantly, in the lanes containing the untreated immunoconjugates, fluorescence signal can *only* be observed in the band representing the heavy chain. Even more convincingly, a *complete* loss of fluorescence can be observed for the heavy chain bands of the PNGaseF-treated immunoconjugates (*Fig. S1 and S2*).

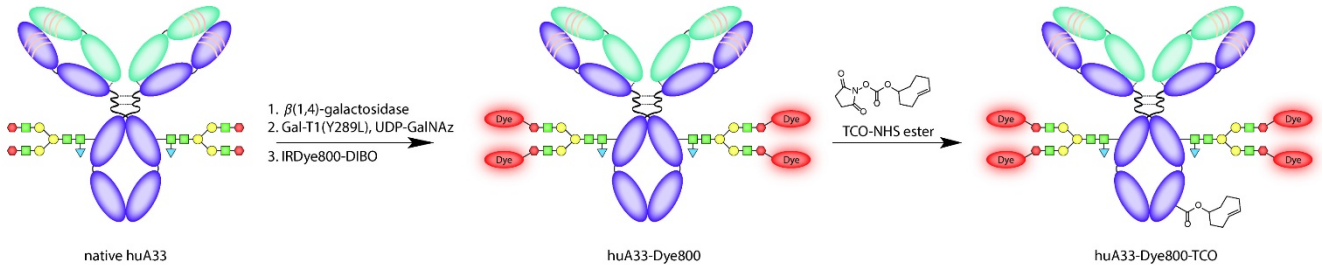

Figure 3. Schematic of the synthesis of huA33-Dye800-TCO.

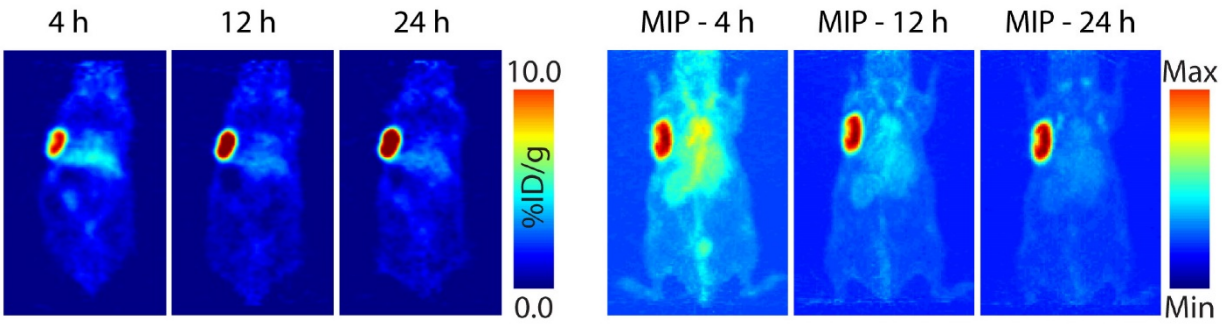

Figure 4. Planar (left) and maximum intensity projection (MIP; right) pretargeted PET images of a nude mouse bearing subcutaneous SW1222 xenograft on the left shoulder. The mouse was injected with huA33-Dye800-TCO (100 μg; 0.66 nmol), followed 48 h later by ^{64}Cu-Tz-SarAr (350-400 μCi; 0.66-0.77 nmol). The coronal slices intersect the center of the tumors.

Next, in line with previously reported procedures, TCO moieties were grafted to the huA33-Dye800 immunoconjugate through the coupling of NHS ester-bearing TCOs to the lysine residues of the antibody. The site-specific conjugation of TCO via a dual labeling approach similar to that which we have recently published was considered.[18,27] However, we did not want the degree of labeling of TCO to be impacted by the presence of Dye800 *or* limited by the availability of the four azide-modified monosaccharides. Ultimately, the conjugation of TCO-NHS to huA33-TCO yielded the completed huA33-Dye800-TCO conjugate after purification via size exclusion chromatography.[23] Quantification of the number of active TCO moieties attached to the antibody was achieved via UV-Vis spectrophotometry following the reaction of huA33-Dye800-TCO with a tetrazine-bearing fluorescent probe: Tz-PEG$_7$-AF488. A degree of labeling of 3.0 ± 0.5 active TCOs/mAb was obtained. Finally, in order to assess the impact of the two bioconjugations on the affinity of the antibody for its target, an antigen binding assay was performed using A33 antigen-expressing SW1222 human colorectal carcinoma cells. The ^{64}Cu-labeled radioimmunoconjugate — obtained via the *ex vivo* reaction of huA33-Dye800-TCO and ^{64}Cu-Tz-SarAr and subsequent size exclusion chromatography — possessed an immunoreactive fraction of 0.90 ± 0.03.

In Vivo PET Imaging and Biodistribution

The *in vivo* performance of pretargeted imaging with huA33-Dye800-TCO and ^{64}Cu-Tz-SarAr was next evaluated in mice bearing subcutaneous A33 antigen-expressing SW1222 colorectal carcinoma xenografts. To this end, huA33-Dye800-TCO (100 μg; 0.66 nmol) was administered intravenously to the tumor-bearing mice followed — after a 48 hour pretargeting interval — by ^{64}Cu-Tz-SarAr (350-400 μCi; 0.66-0.77 nmol). Previous work by our laboratories has illustrated that this 48-hour interval produces high tumor-to-background activity concentration ratios as well as high absolute activity concentrations in the tumor tissue itself.[28]

PET images were collected 4, 12, and 24 h after the administration of the radioligand (*Fig. 4, Fig. S3*). The images acquired at the earliest time point clearly illustrate that this system is capable of the rapid and high contrast visualization of tumor tissue. The images improve with time, with the tumor far and away the organ with the highest activity concentration by 12 and 24 h post-injection. Biodistribution experiments mirrored the observations made during PET imaging (*Table 1*). At 1 h post-injection, the activity concentration in the tumor is 5.6 ± 1.4 %ID/g, a value which grows to 12.8 ± 2.2 %ID/g by 24 h. Over the same time period, the activity in the blood drops from 6.9 ± 2.1 %ID/g to 2.6 ± 0.6 %ID/g. By the later time points, all healthy organs except for the kidneys have activity concentrations below — and often *well* below — 1.9 %ID/g. The kidneys were the non-target organs with the highest activity concentrations (3.9 ± 0.6 %ID/g

and 2.1 ± 0.2 %ID/g at 1 and 24 h, respectively), a result of the renal elimination of excess, 'unclicked' ^{64}Cu-Tz-SarAr radioligand.

Table 1. Biodistribution data for in vivo pretargeting with huA33-Dye800-TCO and ^{64}Cu-Tz-SarAr.

	1 h	4 h	12 h	24 h
Blood	6.9 ± 2.1[a]	5.5 ± 0.9	5.3 ± 0.5	2.6 ± 0.6
Tumor	5.6 ± 1.4	8.0 ± 1.5	15.6 ± 1.7	12.8 ± 2.2
Heart	2.7 ± 0.8	2.2 ± 0.5	2.1 ± 0.3	1.1 ± 0.2
Lung	3.4 ± 1.5	3.7 ± 0.7	3.3 ± 0.2	1.6 ± 0.3
Liver	2.7 ± 0.8	2.6 ± 0.4	2.2 ± 0.2	1.9 ± 0.4
Spleen	1.6 ± 0.7	1.3 ± 0.4	1.3 ± 0.2	1.2 ± 0.3
Stomach	0.6 ± 0.2	0.4 ± 0.1	0.3 ± 0.1	0.3 ± 0.1
Small Intestine	1.0 ± 0.4	0.6 ± 0.1	0.6 ± 0.1	0.5 ± 0.1
Large Intestine	0.5 ± 0.2	0.8 ± 0.2	0.4 ± 0.1	0.4 ± 0.2
Kidney	3.9 ± 0.6	3.2 ± 0.1	2.9± 0.3	2.1 ± 0.2
Muscle	0.5 ± 0.3	0.5 ± 0.1	0.6 ± 0.1	0.3 ± 0.1
Bone	0.8 ± 0.3	0.6 ± 0.1	0.8 ± 0.2	0.6 ± 0.1

[a]Values are %ID/g ± SD. Mice (n = 4) bearing subcutaneous SW1222 xenografts were administered huA33-Dye800-TCO (100 μg; 0.66 nmol) via tail vein injection. After 48 h, the same mice were administered ^{64}Cu-Tz-SarAr (300-400 μCi; 0.66-0.77 nmol), also via tail vein injection. Stomach, small intestine, and large intestine values include contents.

These biodistribution results underscore some intriguing differences between this multimodal pretargeting system and our previously published PET-only pretargeting strategy based on huA33-TCO and ^{64}Cu-Tz-SarAr.[28] In experiments using a 48 h pretargeting interval, the latter system yielded a tumoral activity concentration of 4.5 ± 0.4 %ID/g at 1 h post-injection, a value which did not appreciably change over the course of 24 h (4.9 ± 0.7 %ID/g at 24 h). This strongly suggests that the vast majority of *in vivo* click ligations occurred at the tumor rather than in the blood. In this multimodal pretargeting system, high activity concentrations (5.6 ± 1.4 %ID/g) can be observed in the tumor at 1 h post-injection, which is also indicative of significant click ligations at the tumor site. However, in this case, the activity concentrations in the tumor *increase* over the course of the experiment, ultimately reaching 12.8 ± 2.2 %ID/g at 24 h. The activity concentrations in the blood are also higher for the multimodal approach than the PET-only strategy: at 4 h post-injection, for example, the former produces a blood activity concentration of 5.5 ± 0.8 %ID/g compared to a value of 1.8 ± 0.3 %ID/g for the latter. These data suggest that in the multimodal system, an appreciable amount of 'in-blood' ligations are occurring in addition to the 'on-tumor' reactions. The most likely explanation for this phenomenon is that the addition of the hydrophobic and bulky NIR fluorophore alters the pharmacokinetics of the immunoconjugate, giving the huA33-Dye800-TCO construct a longer blood half-life than its singly modified huA33-TCO cousin. Ultimately, this issue is not a problem, per se. However, it does suggest that longer pretargeting intervals may be necessary to maximize the dosimetric benefits of this imaging system. Indeed, a pilot imaging study using a 96 h pretargeting interval hints that this is the case: the activity concentrations in the blood are lower throughout the experiment, and the activity concentration in the tumor are very similar at 4 and 24 h post-injection (*Fig. S4*). In the end, though, it is important to note that even with these slightly elevated activity concentrations in the blood, this multimodal pretargeting strategy produces promising tumor-to-non-target tissue activity concentration ratios. For example, at 24 h post-injection, the tumor-to-blood and tumor-to-muscle activity concentration ratios are ~5 and ~42, respectively (*Table S1*). Even more importantly, the tumor-to-organ activity concentration ratios for the site of primary tumors (the large intestine) and the most likely site of metastatic disease (the liver) are also high: ~33 and ~7, respectively.

In Vivo NIRF Imaging

The PET and biodistribution results strongly suggest that this system could be highly effective for the image-guided resection of tumor tissue. To explore this possibility, NIRF imaging (λ_{ex} = 745 nm; λ_{em} = 820 nm) was performed on the mice of the PET imaging cohort immediately before the administration of the ^{64}Cu-Tz-SarAr radioligand as well as 24 and 48 h thereafter (and thus 48, 72, and 96 h after the injection of huA33-Dye800-TCO; *see Fig. 2B for a temporal scheme*). The *in vivo* fluorescence images clearly illustrate the specific localization of huA33-Dye800-TCO to the subcutaneous xenografts (*Fig. S5 and Fig. 5A*). Simulated tumor resections further illustrate the potential of this approach for image-guided surgery. After the removal of the skin above the fluorescent area, the NIRF signal increases, and the tumor margins appear clearly, facilitating the excision of all the tumor tissue (*Fig. 5B*). NIRF imaging of the mice *after* the removal of the tumor clearly shows that there is no more fluorescent tissue in the surgical cavity, confirming the complete resection of the lesion. Finally, the tumors and a selection of 8 organs were excised and compared via *ex vivo* NIRF imaging (*Fig. 5C*). These images and the accompanying radiant efficiency values reinforce the specific and selective targeting of this system (*Fig. 5D; for more examples, see Fig. S6-S7*). The tumor tissue has a radiant efficiency of 1393.0 ± 46.0 (units = 10^6 photons·sec^{-1}·cm^{-2}·sr^{-1}/μW·cm^{-2}), a value over an order of magnitude greater than that of the heart (32.5 ± 3.4), lungs (37.0 ± 0.7), liver (107.5 ± 14.0), small

intestine (54.5 ± 18.4), large intestine (35.9 ± 5.3), and kidneys (52.0 ± 2.6) (see *Table S2*). As a result, the tumor-to-liver radiant efficiency ratio is 13, and the corresponding ratios for all of the other healthy organs were >22, including a particularly promising tumor-to-large intestine radiant efficiency ratio of >38.

Histology and Autoradiography

The subcutaneous xenografts from the mice of the PET and NIRF imaging cohort were excised in order to further study the microscopic distribution of the radioligand and fluorophore (*Fig. 6*). Staining for the A33 glycoprotein reveals a clear co-localization between the expression of the A33 antigen and the fluorescence of Dye800, which could only be detected in areas corresponding to tumor cells and not vasculature, necrosis, or stroma. Most importantly, autoradiographical analysis reveals that the radiotracer can only be observed in areas where the Dye800-fluorescence signal is *also* detected, providing further evidence for the *in vivo* formation of the ^{64}Cu-SarAr-huA33-Dye800 radioimmunoconjugate.

In Vivo Multimodal Imaging in Alternative Murine Models of Colorectal Cancer

In order to more fully characterize the *in vivo* performance of this multimodal imaging system, we also performed experiments using peritoneal and patient-derived colorectal cancer xenografts. With regard to the former, SW1222 human colorectal carcinoma cells were injected into the peritoneum of athymic nude mice. After 3-4 weeks, pretargeted PET imaging with huA33-Dye800-TCO and ^{64}Cu-Tz-SarAr clearly revealed small peritoneal tumors while producing minimal activity concentrations in the surrounding non-target tissues (*Fig. 7A*). Subsequent NIRF imaging confirmed the presence of these lesions and enabled the image-guided removal of the tumor tissue (*Fig. 7C*). Interestingly, in one mouse, the NIRF imaging revealed the presence of extremely small (<1 mm) colorectal metastases that had escaped detection *via* PET, mostly likely due to the higher resolution of NIRF imaging compared to microPET imaging.

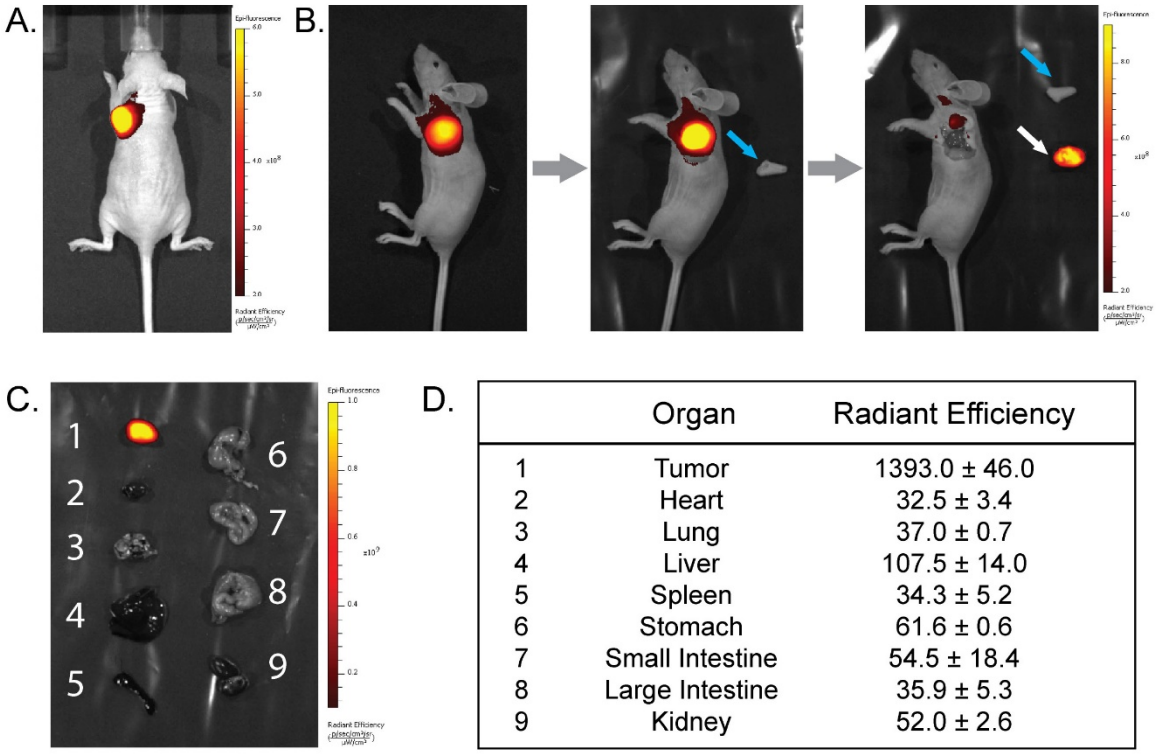

	Organ	Radiant Efficiency
1	Tumor	1393.0 ± 46.0
2	Heart	32.5 ± 3.4
3	Lung	37.0 ± 0.7
4	Liver	107.5 ± 14.0
5	Spleen	34.3 ± 5.2
6	Stomach	61.6 ± 0.6
7	Small Intestine	54.5 ± 18.4
8	Large Intestine	35.9 ± 5.3
9	Kidney	52.0 ± 2.6

Figure 5. (A) Near-infrared fluorescence images (λ_{ex} = 745 nm; λ_{em} = 820 nm) of a mouse bearing a subcutaneous SW1222 xenograft on the left shoulder acquired 2 h after the injection of huA33-Dye800-TCO and 48 h after the subsequent administration of ^{64}Cu-Tz-SarAr. (B) Simulated image-guided resection of the tumor 96 h after the injection of huA33-Dye800-TCO. From left to right: intact mouse, mouse after removal of the skin (blue arrow) covering the tumor, and mouse after excision of the tumor (white arrow). (C) Fluorescence imaging of a selection of organs (1: tumor, 2: heart, 3: lungs, 4: liver, 5: spleen, 6: stomach, 7: small intestine, 8: large intestine, 9: kidneys). (D) Ex vivo radiant efficiencies (in 10^6 photons·sec^{-1}·cm^{-2}·sr^{1}/μW·cm^{-2}) of a selection of organs.

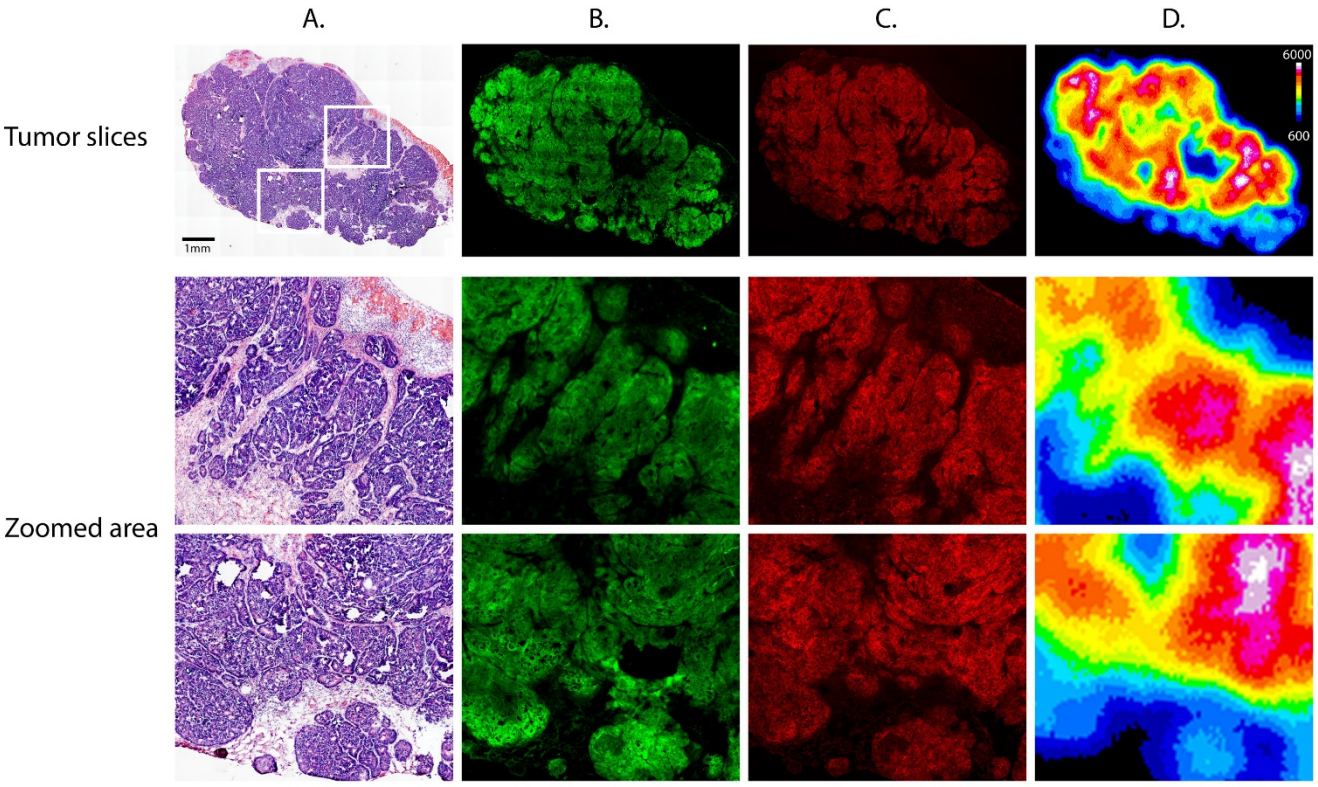

Figure 6. Tumor slices excised from a mouse 72 hours after injection of huA33-Dye800-TCO (100 μg; 0.66 nmol) and 24 h after administration of ^{64}Cu-Tz-SarAr (350-400 μCi; 0.66-0.77 nmol). Upper section: (A) Hematoxylin and eosin staining, (B) immunofluorescence staining for the A33 antigen, (C) confocal fluorescence of the Dye800 signal, and (D) digital autoradiography. Lower section: magnified areas of the tumor slices corresponding to the white boxes in the top left panel.

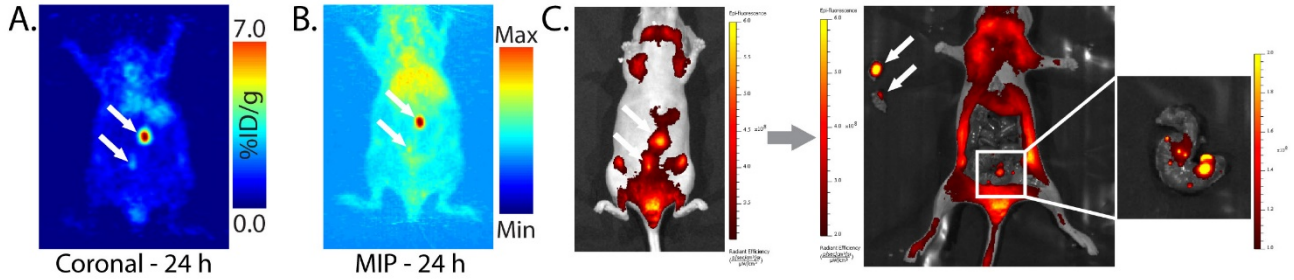

Figure 7. Planar (A) and maximum intensity projection (MIP; B) pretargeted PET images of a nude mouse bearing peritoneal SW1222 tumors (white arrows). The mouse was injected with huA33-Dye800-TCO (100 μg; 0.66 nmol), followed 48 h later with ^{64}Cu-Tz-SarAr (350-400 μCi; 0.66-0.77 nmol). The coronal slice intersects the center of the tumors. (C) Simulated NIRF-guided resection of the tumor 96 h after the injection of huA33-Dye800-TCO (and thus 48 h after the injection of ^{64}Cu-Tz-SarAr; λ_{ex} = 745 nm and λ_{em} = 820 nm). From left to right: NIRF image of the tumors (black arrows) under the skin; NIRF image of the mouse after the excision of the two tumor masses; inset image of the colon, revealing small tumor lesions visible only via NIRF imaging.

Finally, pretargeted PET/NIRF imaging of mice bearing patient-derived colorectal cancer xenografts (PDXs) produced similarly promising results (*Fig. 8*). Indeed, both the PET and NIRF image contrast between the malignant tissue and healthy organs proved to be more than sufficient for the non-invasive visualization of the tumor and its efficient image-guided resection. Interestingly, however, the tumor-to-blood activity concentration ratios seemed to be quite a bit higher in these experiments than in those using SW1222-based xenografts. The most likely explanation for this phenomenon is that while the same amount of Dye800-huA33-TCO (100 μg) was injected for the imaging experiments in both models, the PDXs do not express the A33 antigen at levels comparable to their SW1222 xenograft counterparts. This would naturally result in decreased amounts of Dye800-huA33-TCO in the tumor, increased amounts of Dye800-huA33-TCO in the blood, and a higher proportion of *in vivo* click ligations with ^{64}Cu-Tz-SarAr that occurs in the blood.

Dosimetry

Finally, the biodistribution data from the experiments using subcutaneous SW1222 xenografts were used to perform dosimetry calculations to probe

the dosimetric benefits of pretargeting with huA33-Dye800-TCO and ^{64}Cu-Tz-SarAr (see *Table S3*). These calculations reveal that the total effective dose for this multimodal pretargeting strategy is 0.021 mSv/MBq, an over 20-fold reduction compared to that created by the most *clinically relevant* alternative: huA33 directly labeled with ^{89}Zr (^{89}Zr-DFO-huA33; 0.416 mSv/MBq).[23] This dosimetric advantage grows when considering particularly radiosensitive organs such as the red marrow (40-fold difference), osteogenic cells (30-fold difference), and kidneys (33-fold difference). Admittedly — and not surprisingly, given our previous discussion of the biodistribution data — this multimodal strategy has a slightly *higher* effective dose (0.021 mSv/MBq) than our PET-only system (0.012 mSv/MBq), most likely due to the increased activity concentrations in the blood.

Conclusion

In the preceding pages, we have presented the development and *in vivo* validation of a pretargeted approach to the multimodal PET/NIRF imaging of colorectal carcinoma. In subcutaneous, peritoneal, and patient-derived xenograft models, we have shown that this technology enables both the non-invasive visualization of malignant lesions *and* the NIRF-guided excision of tumor tissue. As a result, we contend that this technology could offer an effective alternative to multimodal imaging with directly radiolabeled antibodies that lowers the total effective radiation dose to patients and reduces the lag time between PET imaging and surgery. Moving forward, we plan on pursuing three different avenues for the optimization of this approach: (1) the use of longer pretargeting intervals (*e.g.* 96 or 120 h) that will reduce the amount of immunoconjugate remaining in the blood at the injection of the radioligand; (2) the use of tetrazine-bearing clearing agents to remove residual immunoconjugate in the blood after the pretargeting interval; and (3) the use of radioligands bearing even shorter-lived radioisotopes such as ^{68}Ga ($t_{1/2}$ = 68 min) and ^{18}F ($t_{1/2}$ = 110 min).[21,26,45,46] We believe that each of these steps could improve upon the already significant advantages that this system provides over imaging with traditional radioimmunoconjugates. Indeed, all three alterations could lead to additional reductions in the effective radiation dose created by this system, and the third could further reduce the necessary interval between

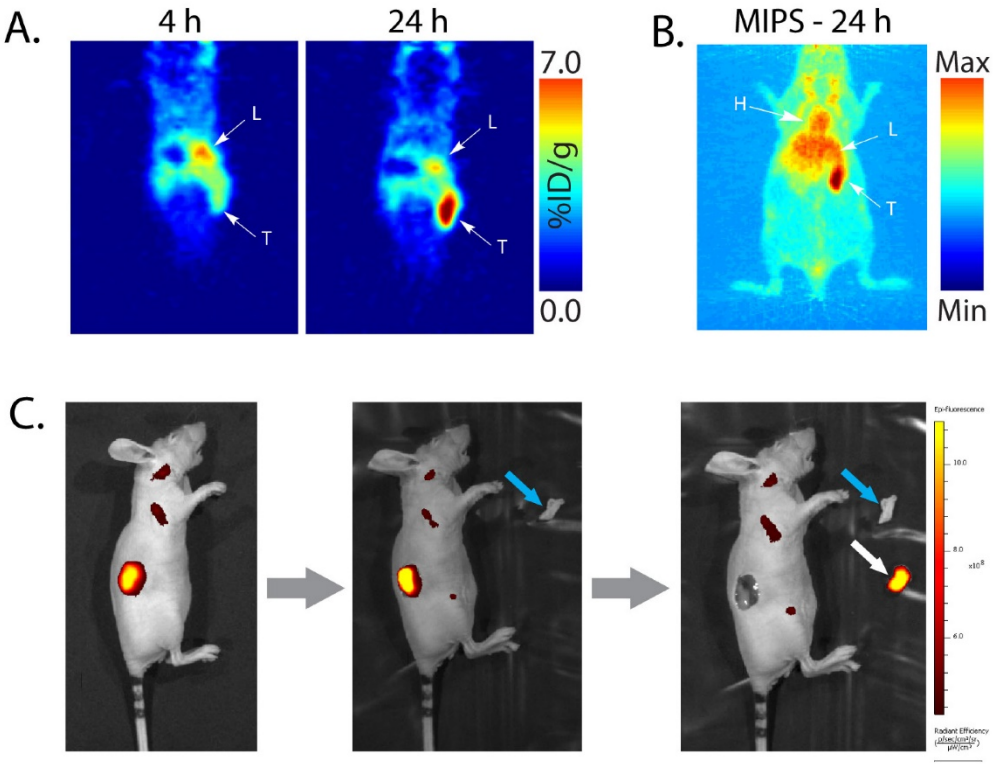

Figure 8. Planar (A) and maximum intensity projection (MIP; B) pretargeted PET images of a nude mouse bearing a patient-derived colorectal carcinoma xenograft (T: tumor, L: liver, H: heart). The mouse was injected with huA33-Dye800-TCO (100 μg; 0.66 nmol), followed 48 h later with ^{64}Cu-Tz-SarAr (350-400 μCi; 0.66-0.77 nmol). The coronal slices intersect the center of the tumor. (C) Simulated image-guided resection of the tumor 96 h after the injection of huA33-Dye800-TCO (and thus 48 h after the administration of ^{64}Cu-Tz-SarAr). From left to right: intact mouse, mouse after removal of the skin (blue arrow) covering the tumor, and mouse after excision of the tumor (white arrow).

PET and surgery. Along these lines, we are currently working to develop pretargeted PET/NIRF imaging systems that leverage the Al^{18}F-labeled tetrazine radioligands that our laboratories have recently reported as well as a series of novel ^{68}Ga-labeled tetrazines. Ultimately, it is our sincere hope that this new multimodal imaging technology will have a significant impact on both the staging and surgical intervention of patients with colorectal carcinoma.

Supplementary Material

Supplementary tables and figures.
http://www.thno.org/v06p2267s1.pdf

Acknowledgements

Services provided by the MSKCC Small-Animal Imaging Core Facility were supported in part by NIH grants R24 CA83084 and P30 CA08748. The authors are also grateful for the generous financial support of the National Institutes of Health (4R00CA178205-02; BMZ), the TeamConnor Childhood Cancer Foundation (BMZ), the National Institute on Minority Health and Health Disparities (G12MD007599; BMZ), the Tow Foundation Fellowship Program in Molecular Imaging and Nanotechnology (JSL; BEC), and Mr. William H. Goodwin and Mrs. Alice Goodwin and the Commonwealth Foundation for Cancer Research and The Center for Experimental Therapeutics at Memorial Sloan Kettering Cancer Center (JSL). We would also like to thank Dr. Elisa De Stanchina for her assistance in the production of the patient-derived xenograft model of colorectal cancer.

Competing Interests

The authors have declared that no competing interest exists.

References

1. Ferlay J, Shin H-R, Bray F, *et al.* Estimates of worldwide burden of cancer in 2008: GLOBOCAN 2008. Int J Cancer. 2010; 127: 2893–2917.
2. DeSantis CE, Lin CC, Mariotto AB, *et al.* Cancer treatment and survivorship statistics, 2014. CA: A Cancer J Clin. 2014; 64: 252–271.
3. Honein-AbouHaidar GN, Kastner M, Vuong V, *et al.* Benefits and barriers to participation in colorectal cancer screening: a protocol for a systematic review and synthesis of qualitative studies. BMJ Open. 2014; 4: e004508.
4. Simillis C, Hompes R, Penna M, *et al.* A systematic review of transanal total mesorectal excision. Is this the future of rectal cancer surgery? Colorectal Dis. 2015; 18:19-39.
5. Kim YW & Kim IY. The role of surgery for asymptomatic primary tumors in unresectable stage IV colorectal cancer. Ann Coloproctology. 2013; 29: 44–54.
6. Mella J, Biffin A, Radcliffe AG, *et al.* Population-based audit of colorectal cancer management in two UK health regions. Br J Surg. 1997; 84: 1731–1736.
7. Nordic Gastrointestinal Tumor Adjuvant Therapy Group. Expectancy or primary chemotherapy in patients with advanced asymptomatic colorectal cancer: a randomized trial. J Clin Oncol. 1992; 10: 904–911.
8. Wu AM & Olafsen T. Antibodies for molecular imaging of cancer. Cancer J. 2008; 14: 191–197.
9. Frangioni JV. In vivo near-infrared fluorescence imaging. Curr Opin Chem Biol. 2003; 7: 626–634.
10. te Velde EA, Veerman T, Subramaniam V, *et al.* The use of fluorescent dyes and probes in surgical oncology. Eur J Surg Oncol. 2010; 36: 6–15.
11. Seibold U, Wängler B, Schirrmacher R, *et al.* Bimodal imaging probes for combined PET and OI: recent developments and future directions for hybrid agent development. BioMed Res Int. 2014; 2014: 153741.
12. Sampath L, Kwon S, Ke S, *et al.* Dual-labeled trastuzumab-based imaging agent for the detection of human epidermal growth factor receptor 2 overexpression in breast cancer. J Nucl Med. 2007; 48: 1501–1510.
13. Paudyal P, Paudyal B, Iida Y, *et al.* Dual functional molecular imaging probe targeting CD20 with PET and optical imaging. Oncol Rep. 2009; 22: 115–119.
14. Sampath L, Kwon S, Hall MA, *et al.* Detection of cancer metastases with a dual-labeled near-infrared/positron emission tomography imaging agent. Transl Oncol. 2010; 3: 307–317.
15. Hong H, Zhang Y, Severin GW, *et al.* Multimodality imaging of breast cancer experimental lung metastasis with bioluminescence and a monoclonal antibody dual-labeled with ^{89}Zr and IRDye 800CW. Mol Pharm. 2012; 9: 2339–2349.
16. Zhang Y, Hong H, Severin GW, *et al.* ImmunoPET and near-infrared fluorescence imaging of CD105 expression using a monoclonal antibody dual-labeled with ^{89}Zr and IRDye 800CW. Am J Transl Res. 2012; 4: 333.
17. Cohen R, Vugts DJ, Walsum MS, *et al.* Inert coupling of IRDye800CW and zirconium-89 to monoclonal antibodies for single- or dual-mode fluorescence and PET imaging. Nat Protoc. 2013; 8: 1010–1018.
18. Zeglis BM, Davis CB, Abdel-Atti D, *et al.* Chemoenzymatic strategy for the synthesis of site-specifically labeled immunoconjugates for multimodal PET and optical imaging. Bioconjug Chem. 2014; 25: 2123–2128.
19. van de Watering FCJ, Rijpkema M, Robillard M, *et al.* Pretargeted imaging and radioimmunotherapy of cancer using antibodies and bioorthogonal chemistry. Nucl Med. 2014; 1: 44.
20. Rossin R, Renart Verkerk P, van den Bosch SM, *et al. In vivo* chemistry for pretargeted tumor imaging in live mice. Angew Chem Int Ed. 2010; 49: 3375–3378.
21. Rossin R, Läppchen T, Bosch SM van den, *et al.* Diels–Alder reaction for tumor pretargeting: *in vivo* chemistry can boost tumor radiation dose compared with directly labeled antibody. J Nucl Med. 2013; 54: 1989–1995.
22. Rossin R, van den Bosch SM, ten Hoeve W, *et al.* Highly reactive trans-cyclooctene tags with improved stability for Diels–Alder chemistry in living systems. Bioconjug Chem. 2013; 24: 1210–1217.
23. Zeglis BM, Sevak KK, Reiner T, *et al.* A pretargeted PET imaging strategy based on bioorthogonal Diels–Alder click chemistry. J Nucl Med. 2013; 54: 1389–1396.
24. Reiner T & Zeglis BM. The inverse electron demand Diels–Alder click reaction in radiochemistry. J Label Compd Radiopharm. 2014; 57: 285–290.
25. Devaraj NK & Weissleder R. Biomedical applications of tetrazine cycloadditions. Acc Chem Res. 2011; 44: 816–827.
26. Devaraj NK, Thurber GM, Keliher EJ, *et al.* Reactive polymer enables efficient in vivo bioorthogonal chemistry. Proc Natl Acad Sci. 2012; 109: 4762–4767.
27. Cook BE, Adumeau P, Membreno R, *et al.* Pretargeted PET imaging using a site-specifically labeled immunoconjugate. Bioconjug Chem. 2016;
28. Zeglis BM, Brand C, Abdel-Atti D, *et al.* Optimization of a pretargeted strategy for the PET imaging of colorectal carcinoma via the modulation of radioligand pharmacokinetics. Mol Pharm. 2015; 12: 3575–3587.
29. Houghton JL, Zeglis BM, Abdel-Atti D, *et al.* Site-specifically labeled CA19.9-targeted immunoconjugates for the PET, NIRF, and multimodal PET/NIRF imaging of pancreatic cancer. Proc Natl Acad Sci. 2015; 112: 15850–15855.
30. Welt S, Scott AM, Divgi CR, *et al.* Phase I/II study of iodine 125-labeled monoclonal antibody A33 in patients with advanced colon cancer. J Clin Oncol. 1996; 14: 1787–1797.
31. Sakamoto J, Kojima H, Kato J, *et al.* Organ-specific expression of the intestinal epithelium-related antigen A33, a cell surface target for antibody-based imaging and treatment in gastrointestinal cancer. Cancer Chemother Pharmacol. 2000; 46: S27–S32.
32. Scott AM, Lee F-T, Jones R, *et al.* A phase I trial of humanized monoclonal antibody A33 in patients with colorectal carcinoma: biodistribution, pharmacokinetics, and quantitative tumor uptake. Clin Cancer Res. 2005; 11: 4810–4817.
33. Sakamoto J, Oriuchi N, Mochiki E, *et al.* A phase I radioimmunolocalization trial of humanized monoclonal antibody huA33 in patients with gastric carcinoma. Cancer Sci. 2006; 97: 1248–1254.
34. Carrasquillo JA, Pandit-Taskar N, O'Donoghue JA, *et al.* ^{124}I-huA33 antibody PET of colorectal cancer. J Nucl Med. 2011; 52: 1173–1180.
35. Ackerman ME, Chalouni C, Schmidt MM, *et al.* A33 antigen displays persistent surface expression. Cancer Immunology, Immunother. 2008; 57: 1017–1027.
36. Adumeau P, Sharma SK, Brent C, *et al.* Site-specifically labeled immunoconjugates for molecular imaging—Part 1: cysteine residues and glycans. Mol Imaging Biol. 2016; 18: 1–17.
37. Adumeau P, Sharma SK, Brent C, *et al.* Site-specifically labeled immunoconjugates for molecular imaging—Part 2: peptide tags and unnatural amino acids. Mol Imaging Biol. 2016; 18: 153–165.
38. Agarwal P & Bertozzi CR. Site-specific antibody–drug conjugates: the nexus of bioorthogonal chemistry, protein engineering, and drug development. Bioconjug Chem. 2015; 26: 176–192.
39. Behrens CR & Liu B. Methods for site-specific drug conjugation to antibodies. mAbs. 2014; 6: 46–53.
40. Ramakrishnan B & Qasba PK. Structure-based design of β1,4-galactosyltransferase I (β4Gal-T1) with equally efficient *N*-acetylgalactosaminyltransferase activity. J Biol Chem. 2002; 277: 20833–20839.

41. Khidekel N, Arndt S, Lamarre-Vincent N, *et al.* A chemoenzymatic approach toward the rapid and sensitive detection of O-GlcNAc post-translational modifications. J Am Chem Soc. 2003; 125: 16162–16163.
42. Boeggeman E, Ramakrishnan B, Kilgore C, *et al.* Direct identification of non-reducing GlcNAc residues on *N*-glycans of glycoproteins using a novel chemoenzymatic method. Bioconjug Chem. 2007; 18: 806–814.
43. Boeggeman E, Ramakrishnan B, Pasek M, *et al.* Site-specific conjugation of fluoroprobes to the remodeled Fc *N*-glycans of monoclonal antibodies using mutant glycosyltransferases: application for cell surface antigen detection. Bioconjug Chem. 2009; 20: 1228–1236.
44. Zeglis BM, Davis CB, Aggeler R, *et al.* Enzyme-mediated methodology for the site-specific radiolabeling of antibodies based on catalyst-free click chemistry. Bioconjug Chem. 2013; 24: 1057–1067.
45. Evans HL, Carroll L, Aboagye EO, *et al.* Bioorthogonal chemistry for ^{68}Ga radiolabelling of DOTA-containing compounds. J Label Compd Radiopharm. 2014; 57: 291–297.
46. Zhu J, Li S, Wängler C, *et al.* Synthesis of 3-chloro-6-((4-(di-tert-butyl[^{18}F]fluorosilyl)-benzyl)oxy)-1,2,4,5-tetrazine ([^{18}F]SiFA-OTz) for rapid tetrazine-based ^{18}F-radiolabeling. Chem Comm. 2015; 51: 12415–12418.